Preprints of the 18th IFAC World Congress
Milano (Italy) August 28 - September 2, 2011

Analytical Multi-Point Trajectory Generation for Differentially Flat Systems with Output Constraints

Thomas Ruppel * **Karl Lukas Knierim** * **Oliver Sawodny** *

* *Institute for System Dynamics, University of Stuttgart, Germany*
(e-mail: thomas.ruppel@isys.uni-stuttgart.de).

Abstract: In this paper, an analytical off-line multi-point trajectory generation scheme is presented for differentially flat systems. For control of dynamical systems along a given set of control points, multi-point trajectory generation is required when input and state constraints exist. It is assumed that differential constraints for flat coordinates can be formulated explicitly. The trajectory scheme is based on analytically solving a set of polynomial equations to parameterize n-times continuously differentiable segmented transition polynomials, that approximate time optimal trajectories. The computational effort for determining valid trajectories is low in comparison to numerical optimization. As an example, a multi-point trajectory generation problem for a 3-DOF gantry crane is presented.

Keywords: Application of mechatronic principles; Identification and control methods; Mechatronic systems

1. INTRODUCTION

Feedforward control is widely used in control applications as an extension of feedback control to separately design tracking performance by the feedforward part and closed-loop stability and robustness by the feedback part.

A key element in feedforward control is the trajectory generator Σ^* (Fig. 1) providing continuously differentiable trajectories along given points. Based on the task specification, motion planning requires either planning a temporal trajectory along a predefined path or planning both a path and a trajectory. While a path is specified by points in Cartesian space (or in joint space) describing a spatial evolution of an end-effector (or joints), a trajectory is a curve in state space describing the system evolution in time (Craig, 1989). In this field, a large variety of geometric path planning and dynamic trajectory generation methods have been developed (Choset et al., 2005). The issue of including system dynamics in the path planning process lead to dynamic trajectory planning methods usually referred to as kinodynamic planning (Canny et al., 1991; Donald et al., 1993) as part of motion planning for systems with differential constraints (Fortune and Wilfong, 1988). Over the last decade, apart from solutions by numerical optimization, especially algebraic and trigonometric spline based approaches showed good results (Sciavicco and Siciliano, 2005; Visioli, 2001). However, as soon as constraints for higher time derivatives of the trajectories are included in the trajectory planning, common methods based on algebraic or trigonometric splines must be supported by numerical optimization.

In this paper, it is assumed that a suitable path planning method for finding valid transition points $\boldsymbol{P}_j$ in a configuration space $\mathbb{U}^N \in \mathbb{R}^N$ has been performed already, e.g. by methods described in Latombe (1991) and Lozano-Pérez and Wesley (1979). Geometric preprocessing methods for defining synchronous and asynchronous path segments along given transition points $\boldsymbol{P}_j$ under consideration of geometric constraints can be found in Ruppel et al. (2008).

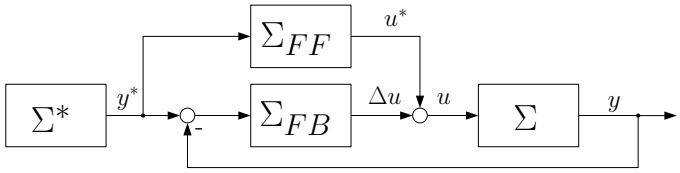

Fig. 1. Structure of the two-degree-of-freedom control scheme with systems Σ, feedback control Σ_{FB}, feedforward control Σ_{FF}, and trajectory generator Σ^*.

In general, independent of the considered system, trajectory generation problems can be reduced to transitions between stationary or non-stationary setpoints within a finite time interval usually including state and input constraints. Mathematically, finding a finite-time transition between stationary setpoints results in a boundary value problem (BVP). The solution of BVPs can either be derived by direct or indirect numerical methods (Keller, 1976; von Stryk and Bulirsch, 1992) or by analytical approaches (Barrère and Carmasol, 1995). This paper will introduce a new set of segmented transition polynomials for solving multi-point boundary value problems analytically. The considered dynamical systems are supposed to be differentially flat (Fliess et al., 1995) such that purely analytical trajectory planning methods can be performed (Graichen et al., 2005). Special attention is drawn to flexibility and scalability of the used ansatz functions to generate n-times continuously differentiable trajectories, where n is a parameter of the trajectory set by the system order. The presented method is focused on off-line trajectory planning that usually occurs for driving mechanical systems including e.g. coordinate measurement machines, multi-axes cranes, or nano-positioning systems.

The outline of this paper is as follows: 1) The system class of differentially flat systems and explicit output constraints are de-

fined. 2) The segmented transition polynomials are derived and scalability is discussed. 3) Methods for time synchronization and implementation for discrete time systems are addressed. 4) The multi-point trajectory generation is presented for the movement of a 3-DOF gantry crane.

2. SYSTEM CLASS

In the following, the multi-axes path planning problem is assumed to be decoupled to independent controllable orthogonal coordinates. This assumption is usually fulfilled for mechanical systems with independently controlled linear axes or appropriately decoupled robotic manipulators. For each controllable axis, the following nonlinear SISO system is considered [1]:

$$\begin{aligned}\Sigma \ : \quad & \dot{\boldsymbol{x}}(t) = \boldsymbol{f}(\boldsymbol{x}(t), u(t)) \ , \ t > 0 \ , \ \boldsymbol{x}(0) = \boldsymbol{x}_0 \in \mathbb{R}^n \\ & y(t) = h(\boldsymbol{x}(t)), \ t \geq 0 \end{aligned} \tag{1}$$

with time $t \in \mathbb{R}^+$, state $\boldsymbol{x} \in \mathbb{R}^n$, control input $u \in \mathbb{R}$, and output $y \in \mathbb{R}$. The vector field $\boldsymbol{f}$: $\mathbb{R}^n \times \mathbb{R} \rightarrow \mathbb{R}^n$ and the function $h : \mathbb{R}^n \rightarrow \mathbb{R}$ are assumed to be sufficiently smooth.

2.1 Transformation to input-output normal form

System (1) can be transformed into the nonlinear input-output normal form Isidori (1995)

$$y^{(r)} = \alpha(y, \dot{y}, \ldots, y^{(r-1)}, \boldsymbol{\eta}, u), \tag{2}$$

$$\dot{\boldsymbol{\eta}} = \boldsymbol{\beta}(y, \dot{y}, \ldots, y^{(r-1)}, \boldsymbol{\eta}, u), \tag{3}$$

with $\alpha(\cdot) = \boldsymbol{L}_f^r h \circ \boldsymbol{\phi}^{-1}$ and $\boldsymbol{\beta}_i(\cdot) = \boldsymbol{L}_f \boldsymbol{\phi}_{\eta,i} \circ \boldsymbol{\phi}^{-1}$. Here, the relative degree r is defined as

$$\frac{\partial}{\partial u}\boldsymbol{L}_f^i h = 0, \ \ i \in \{0, \ldots, r-1\}, \ \ \frac{\partial}{\partial u}\boldsymbol{L}_f^r h \neq 0, \tag{4}$$

with the Lie derivative $\boldsymbol{L}_f$ along the vector field $\boldsymbol{f}$. Moreover, the diffeomorphisms

$$\begin{aligned}(y, \dot{y}, \ldots, y^{(r-1)}, \boldsymbol{\eta}) = \boldsymbol{\phi}(\boldsymbol{x}) \quad & \text{with } \boldsymbol{\eta} = \boldsymbol{\phi}_\eta(\boldsymbol{x}) \in \mathbb{R}^{n-r}, \\ y^{(i)} = \boldsymbol{L}_f^i h(\boldsymbol{x}) = \boldsymbol{\phi}_{i+1}(\boldsymbol{x}), \ \ & i = 0, \ldots, r-1. \end{aligned} \tag{5}$$

are used. For the special case of $r = n$, y is a linearizing or flat output of the system (1) and no internal dynamics exist Fliess et al. (1995). Then, the chain of integrators (2) forms the nonlinear controller normal form

$$\Sigma_{NF} \ : \ y^{(n)} = \overline{\alpha}(y, \dot{y}, \ldots, y^{(n-1)}, u). \tag{6}$$

This structure enables a purely algebraic solution of the transition problem since the feedforward control

$$\Sigma^{-1} \ : \ u^* = \overline{\alpha}^{-1}(y^*, \dot{y}^*, \ldots, y^{*(n)}) \tag{7}$$

can be determined directly in dependence of the desired output trajectory y^* and its first n time derivatives without integration of differential equations. Due to the flatness of system (1), the inverse function $\overline{\alpha}^{-1}$ exists at least locally and (7) describes the relation between the input and the flat output in terms of the inverse system Σ^{-1}, which is used for the implementation of the feedforward control $\Sigma_{FF} = \Sigma^{-1}$ in Fig. 1.

[1] For improved readability, the indices for independent axes are omitted

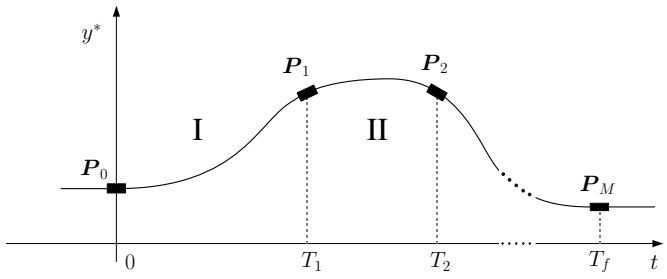

Fig. 2. Desired output trajectory $y^*(t)$ for a transition between multiple target points $\boldsymbol{P}_j$ within the time intervals $t_j \in [T_{j-1}, T_j]$

2.2 Explicit output constraints

For the special case of a maximum relative degree $r = n$, the integrator chain (2) consists of n integrators. It is assumed that the output constraints for system (1) or (2), respectively, can be expressed in terms of upper bounds for each integrator as

$$\| \frac{d^i}{dt^i} y^*(t) \|_\infty \leq c_i \ , \left\{ \boldsymbol{c} \in \mathbb{R}^{n+}, \ i = 1, \ldots, n, \ \ t \in [0, T_f] \right\}. \tag{8}$$

The first three output constraints in (8) are equivalent to requirements for a limitation of velocity, acceleration, and jerk ($n = 3$) of the output trajectory $y^*(t)$ in robotic applications. By use of (7), an upper bound for $u^*(t)$ and upper bounds for time derivatives of $u^*(t)$ can be included implicitly. Constraints on the absolute values of $y^*(t)$ can be included implicitly. For example, $y^*(t) \in [y_0^*, y_f^*] \ \forall t \in [0, T_f]$ is guaranteed by the chosen ansatz function in Section 3.1.

3. TRAJECTORY PLANNING

In order to fulfill the given constraints (8) for the output trajectory $y^*(t)$ and its time derivatives, a time optimal trajectory between boundary conditions $\boldsymbol{P}_j$ using segmented transition polynomials is desired. As shown in Fig. 2, the task is to generate a sufficiently smooth trajectory $y^*(t)$ driving system (1) along given target points $\boldsymbol{P_j} = \{y_j, \dot{y_j}, \ddot{y_j}, 0, \ldots, 0\}, \ j = 0 \ldots M$ under consideration of output constraints (8) in minimal time T_f. Typically, one would expect to set $\dot{y}_j = \ddot{y}_j = 0$ and solve a boundary value problem for a setpoint change $y_j \rightarrow y_{j+1}$ of system (1) Graichen et al. (2005). However, especially in the field of robotics and aeronautics, it is desirable to track a system along recorded points $\boldsymbol{P}_j$ coming from teach-in operation or waypoint specifications. Limiting $\dot{y}_j = \ddot{y}_j = 0$ in $\boldsymbol{P}_j$ would prolong the overall traveling time and reduce the energy efficiency of the trajectory. In the course of this paper, it will be shown that an inclusion of $\dot{y}_j \neq 0$ and $\ddot{y}_j \neq 0$ leads to an algebraic multi-point boundary value problem that can be solved via suitable ansatz functions.

Due to the linear structure of the integrator chain (2), a time optimal solution for a C^n trajectory under output constraints results in switching behavior of the n-th time derivative of $y^*(t)$ Sonneborn and Van Vleck (1964). Planning such trajectories usually leads to numerical optimization of the n-th time derivative of $y^*(t)$, including numerical integration and a strong dependency on the chosen time discretization.

Therefore, it is a common technique to describe the output function $y^*(t)$ by polynomial or trigonometric splines of the form

$$s(t) = \sum_{j=1}^{2n+1} a_j \Xi_j(t), \quad \{a_j \in \mathbb{R},\, t \in [0, T_f]\} \tag{9}$$

with a suitable set of coefficients a_j and basis functions $\Xi_j(t)$ that fulfill the boundary conditions $\boldsymbol{P}_j$. Higher order time derivatives of $s(t)$ can be determined explicitly, but finding a sufficient transition time T_f leads to a set of nonlinear inequalities of the form

$$\| \frac{d^i}{dt^i} s(t) \|_\infty \leq c_i \,, \left\{ \boldsymbol{c} \in \mathbb{R}^{n+},\; i = 1, \ldots, n,\;\; t \in [0, T_f] \right\}. \tag{10}$$

with unknown T_f. Clearly, finding a suitable transition time T_f for arbitrary ansatz functions $\Xi_j(t)$ in (9) and (10) can only be performed numerically since the maximum value of $\frac{d^i}{dt^i} s(t)$ can not be derived directly.

3.1 Segmented transition polynomials

As a new description for the transition function (9), a set of segmented polynomials with a time optimized transition profile for each transition phase $\boldsymbol{P}_j \rightarrow \boldsymbol{P}_{j+1}$ (see Fig. 2) is proposed. The key element in this approach is segmentation since it allows for a purely analytical solution of the transition problem under consideration of output constrains (10). Based on a transition profile described in Ruppel et al. (2008), the proposed segmented transition profile consists of three major stages as shown in Figure 3. The stages are geared to time efficient trajectories for the connection of two stationary or non-stationary setpoints $[\boldsymbol{P}_j, \boldsymbol{P}_{j+1}]$ including:

(1) a stage of constant $\ddot{y}^*(t)$ (acceleration) under consideration of differential constraints (I in Fig. 3),
(2) a stage of constant $\dot{y}^*(t)$ (velocity) with $\ddot{y}^*(t) = 0$ (c in Fig. 3),
(3) a stage of constant $\ddot{y}^*(t)$ (deceleration) under consideration of differential constraints (II in Fig. 3).

The layout and length of each phase depend on the chosen boundary conditions $[\boldsymbol{P}_j, \boldsymbol{P}_{j+1}]$, and the considered system order n ($\boldsymbol{x} \in \mathbb{R}^n$).

To achieve n-times differentiable trajectories, the phases of constant $\ddot{y}^*(t)$ ($I.c$, c, $II.c$) are connected by smooth transition polynomials Piazzi and Visioli (2001) for $\ddot{y}^*(t)$ $\{y^* \in C^n,$ $n \geq 3\}$ of the form

$$\ddot{y}^*_{I1}(t) = \ddot{y}^*_0 + (\ddot{y}^*_{c1} - \ddot{y}^*_0) \cdot \Psi\,(t, T_{1v1}) \tag{11a}$$
$$\ddot{y}^*_{I2}(t) = \ddot{y}^*_{c1} + (\ddot{y}^*_{c} - \ddot{y}^*_{c1}) \cdot \Psi\,(t, T_{1v2}) \tag{11b}$$
$$\ddot{y}^*_{II1}(t) = \ddot{y}^*_{c} + (\ddot{y}^*_{c2} - \ddot{y}^*_{c}) \cdot \Psi\,(t, T_{2v1}) \tag{11c}$$
$$\ddot{y}^*_{II2}(t) = \ddot{y}^*_{c22} + (\ddot{y}^*_{f} - \ddot{y}^*_{c2}) \cdot \Psi\,(t, T_{2v2}) \tag{11d}$$

with the transition polynomial

$$\Psi\,(t, \tau) = \begin{cases} 0 \quad \text{if } \; t \leq 0, \\ \dfrac{(2k+1)!}{k!\tau^{2k+1}} \displaystyle\sum_{i=0}^{k} \frac{(-1)^{k-i}}{i!(k-i)!(2k-i+1)} \tau^i t^{2k-i+1} \\ \qquad\qquad \text{if } \; 0 \leq t \leq \tau \\ 0 \quad \text{if } \; t \geq \tau. \end{cases}, \tag{12}$$

and summation parameter $k = n - 2$. For simplicity, in the following explanation each trajectory segment starts at $t = 0$ and ends at $t = \tau$ [2]. The free parameters in Equations (11a)-(11d) are $\ddot{y}^*_{c1}, \ddot{y}^*_{c2}, T_{1c}, T_c$, and T_{2c}. The parameters $\ddot{y}^*_0$ and $\ddot{y}^*_f$

[2] For a real implementation, a time shift at the corresponding switching points in the trajectory segments must be performed.

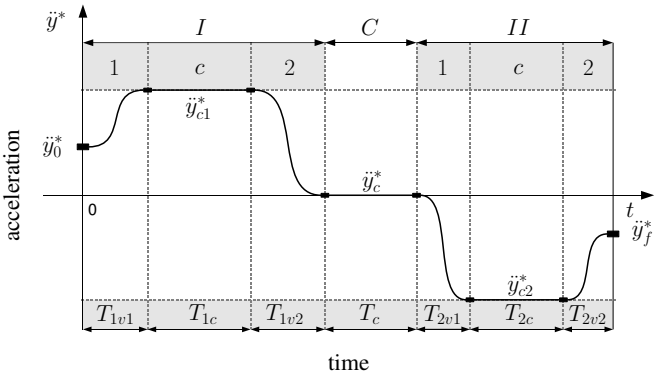

Fig. 3. Segmented transition profile $\ddot{y}^*(t)$ with boundary conditions $\ddot{y}^*(0) = \ddot{y}^*_0,\; \ddot{y}^*(t_f) = \ddot{y}^*_f$.

are predefined by the boundary values $\dot{y}_j$ and $\dot{y}_{j+1}$ in $\boldsymbol{P}_j$ and $\boldsymbol{P}_{j+1}$, respectively. The transition times $T_{1v1},\, T_{1v2}, T_{2v1},\, T_{2v2}$ are determined such that all differential output constraints for $n \geq 3$ are satisfied. Hereby, the symmetric layout of $\Psi(t, \tau)$ allows for an analytical solution of multiples of τ at which $\frac{d^j}{dt^j} \Psi(t, \tau) = 0$, $\{j = 3 \ldots (n-1)\}$. Certainly, one would choose the transition times $T_{1v1}, \ldots, T_{2v2}$ such that one of the differential constraints is reached. Thus, an analytical determination of $T_{1v1}, \ldots, T_{2v2}$ only depends on the output constraints given in (8).

For instance, the transition polynomial for $n = 4$ reads

$$\Psi(t, \tau) = \left(3 \left(\frac{t}{\tau} \right)^2 - 2 \left(\frac{t}{\tau} \right)^3 \right). \tag{13}$$

With (12) and (11a), it follows

$$\begin{aligned} \ddot{\Psi}(t, T_{1v1}) &= 0 \quad \text{for } \; t = 0.5\, T_{1v1}, \\ y^{(3)*}_{I1}(0.5\, T_{1v1}) &= \frac{(\ddot{y}^*_{c1} - \ddot{y}^*_0)}{T_{1v1}} \underbrace{\dot{\Psi}(0.5\, T_{1v1}, T_{1v1})}_{=0.5} \overset{!}{\leq} c_3, \\ T_{1v1} &= \frac{2(\ddot{y}^*_{c1} - \ddot{y}^*_0)}{c_3}, \;\; \text{with } \; \| y^{(3)*}_{I1}(t) \|_\infty \leq c_3. \end{aligned} \tag{14}$$

The inclusion of output constraints for $\ddot{y}^* \leq c_2$ is achieved by limiting $|\ddot{y}^*_{c1}| \leq c_2$ and $|\ddot{y}^*_{c2}| \leq c_2$, respectively.

The determination of T_{1c}, T_{2c} and the fulfillment of boundary conditions for $\dot{y}_j$ and $\dot{y}_{j+1}$ in $\boldsymbol{P}_j$ and $\boldsymbol{P}_{j+1}$ require an examination of the integrals of $\ddot{y}^*(t)$ reading:

$$\dot{y}^*_{I1}(t) = \dot{y}^*_0 + \ddot{y}^*_0 t + (\ddot{y}^*_{c1} - \ddot{y}^*_0) \cdot \int_0^t \Psi\,(t, T_{1v1})\, dt \tag{15a}$$
$$\dot{y}^*_{Ic}(t) = \dot{y}^*_{I1}(T_{1v1}) + \ddot{y}^*_{c1} t \tag{15b}$$
$$\dot{y}^*_{I2}(t) = \dot{y}^*_{Ic}(T_{1c}) + \ddot{y}^*_0 t + (\ddot{y}^*_{c} - \ddot{y}^*_{c1}) \cdot \int_0^t \Psi\,(t, T_{1v2})\, dt \tag{15c}$$
$$\dot{y}^*_{c}(t) = \dot{y}^*_{I2}(T_{1v2}) \tag{15d}$$
$$\dot{y}^*_{II1}(t) = \dot{y}^*_{c}(T_{c}) + \ddot{y}^*_{c} t + (\ddot{y}^*_{c2} - \ddot{y}^*_{c}) \cdot \int_0^t \Psi\,(t, T_{2v1})\, dt \tag{15e}$$
$$\dot{y}^*_{IIc}(t) = \dot{y}^*_{II1}(T_{2v1}) + \ddot{y}^*_{c2} t \tag{15f}$$
$$\dot{y}^*_{II2}(t) = \dot{y}^*_{IIc}(T_{2c}) + \ddot{y}^*_0 t + (\ddot{y}^*_{c} - \ddot{y}^*_{c1}) \cdot \int_0^t \Psi\,(t, T_{2v2})\, dt \tag{15g}$$

Note that the integral $\int_0^\tau \Psi(t, \tau) dt$ is a constant value only depending on the system order n. Thereby, a determination of free parameters in (15a)-(15g) is greatly simplified. Through

(15a)-(15c), it is possible to determine T_{1c} such that $\|\dot{y}_c^*\|_\infty \leq c_1$.

The transition time T_{2c} results from the right boundary condition at $\boldsymbol{P}_{j+1}$ with $\dot{y}_{II2}^* = \dot{y}_f^*$ including (15e)-(15g). The determination of the last transition time T_c can be performed by integration of (15a)-(15g) under consideration of the boundary conditions y_j and y_{j+1} in $\boldsymbol{P}_j$ and $\boldsymbol{P}_{j+1}$, respectively. However, only if the output constraint for $\dot{y}^*$ can be reached during the transition $\boldsymbol{P}_j \rightarrow \boldsymbol{P}_{j+1}$, it is possible to determine T_c analytically. If the maximum velocity $\|\dot{y}^*(t)\|_\infty < c_1$, it is necessary to find a valid value for $\dot{y}_c^*$ numerically because in this case (15a)-(15g) can not be solved analytically anymore.

3.2 Scalability and Application to Discrete Time Systems

Scalability of transition polynomials is required if a synchronization of multiple trajectories (e.g. driving individual robot axes at the same time) and inclusion of path constraints must be achieved. For example, driving a robot manipulator along given points in its configuration space with two or more involved actuators, it is necessary to synchronize either the individual traveling time of all actuators or their dynamic behavior, or both. In this paper, only the general case of equalization of traveling times for multiple trajectories shall be addressed since planning of synchronized dynamic behavior of multiple synchronous trajectories can be reduced to planning of a single trajectory and use of linear projection techniques as described in Ruppel et al. (2008).

It is assumed that all transition times $T_{1v1}, \ldots, T_{2v2}$ of $y^*(t)$ (see Fig. 2) are known for a valid transition $\boldsymbol{P}_j \rightarrow \boldsymbol{P}_{j+1}$ under consideration of output constraints (8) by methods described in Section 3.1. For scaling $y^*(t)$ it is necessary to set the overall traveling time $T_f = T_{1v1} + \ldots + T_{2v2}$ of the transition $\boldsymbol{P}_j \rightarrow \boldsymbol{P}_{j+1}$ to a required transition time $T_r > T_f$. However, compliance with given output constraints has to be assured. Therefore, it is proposed to scale all transition times $T_{1v1}, \ldots, T_{2v2}$ by factor T_r/T_f. A prolongation of all transition times leads to new values for $\ddot{y}_{c1}^*$ and $\ddot{y}_{c2}^*$, which can be calculated through (15a)-(15g) and integrals of (15a)-(15g) by inclusion of the boundary conditions at $\boldsymbol{P}_j$ and $\boldsymbol{P}_{j+1}$. By this seemingly simple method it is possible to adjust multiple trajectories with multiple differential constraints and varying composition of phase segments I, c, and II (see Fig. 2) to the same desired overall traveling time T_r.

Especially in the field of discrete time systems, it can be necessary to account for arbitrary sampling times Δt. These requirements arise when input planning methods as described in Section 3 are used and the control input $u(t)$ in (1) has to be computed directly. However, by planning the flat output trajectory $y^*(t)$ in (7) no numerical integration of the system dynamics is required and thereby no consideration of sampling times is necessary. As a result, the switching times $T_{1v1}, \ldots, T_{2v2}$ do not have to be multiples of the sampling time Δt and only if desired the overall traveling time can be prolonged to a multiple of the sampling time by scaling methods described above.

4. MULTI-POINT TRAJECTORY GENERATION FOR A 3-DOF GANTRY CRANE

To show the applicability of multi-point trajectory generation for differentially flat systems, the movement of a payload in the x-y-plane of a 3-DOF gantry crane is considered. At first, the model of a 3-DOF gantry crane is derived and the flat output is introduced. Afterwards, the feedforward control law is defined and a multi-point trajectory with given boundary conditions along three points is calculated. Finally, experimental results of the payload and trolley transition are presented.

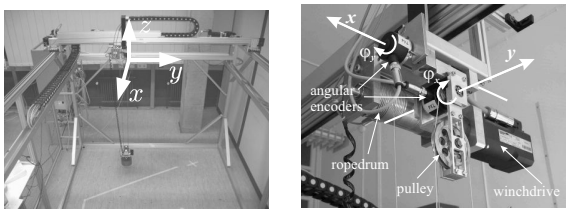

(a) View on experimental setup in $x-$direction. (b) Close up of trolley and cardan joint.

Fig. 4. The setup of an experimental 3-DOF gantry crane.

4.1 Model of a 3-DOF Gantry Crane

An experimental 3-DOF gantry crane is available at the Institute for Systemdynamics (ISYS) Zimmert et al. (2006) (Fig. 4). The gantry crane consists of a moving bridge of mass m_b and a trolley of mass m_t. The trolley is mounted on the bridge and can be moved along the x-direction, whereas the bridge can be moved along the y-direction. The configuration allows for a movement of the trolley within the $x - y$ plane. A payload with mass m_p is connected to the trolley by a rope suspended by a cardan joint. The length of the rope $l(t)$ can be varied by a winch mounted on the trolley. Thereby, the load can be moved in all three dimensions x-y-z. In addition to the measurement of trolley positions $x_t(t)$ and $y_t(t)$, the experimental setup is equipped with encoders to measure the cardan joint angles $\varphi_x(t)$ and $\varphi_y(t)$ (Figure 4(b)). A schematic view of the experimental gantry crane setup is given in Figure 5.

The kinematics of the cardan joint lead to the positions of the load

$$x_p(t) = x_t(t) + l(t)\sin\left(\varphi_x(t)\right) \tag{16a}$$
$$y_p(t) = y_t(t) - l(t)\cos\left(\varphi_x(t)\right)\sin\left(\varphi_y(t)\right) \tag{16b}$$
$$z_p(t) = -l(t)\cos\left(\varphi_x(t)\right)\cos\left(\varphi_y(t)\right). \tag{16c}$$

Neglecting the rope mass and assuming a point mass payload, the kinetic and potential energy of the system reads

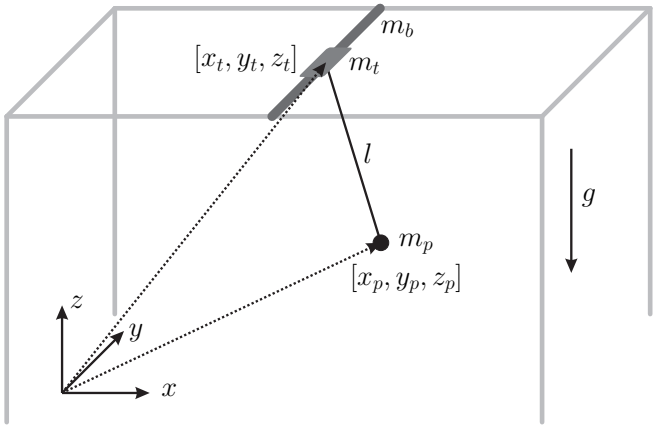

Fig. 5. Schematics of the 3D bridge crane.

$$T = \frac{m_p}{2}\left(\dot{x}_p^2(t) + \dot{y}_p^2(t) + \dot{z}_p^2(t)\right) + \frac{m_t}{2}\left(\dot{x}_t^2(t) + \dot{y}_t^2(t)\right) + \frac{m_b}{2}\dot{x}_t^2(t) \quad (17a)$$

$$V = g m_p z_p(t), \quad (17b)$$

where g denotes the gravity. The inputs to the system are the force $F_y(t)$ applied to the trolley, the force $F_x(t)$ applied to the bridge, and the rope force $F_l(t)$, induced by the winch drive, which results in the virtual work

$$Q(t) = F_y(t)\delta y_t(t) + F_x(t)\delta x_t(t) + F_l(t)\delta l(t). \quad (18)$$

Introducing the generalized coordinates

$$\boldsymbol{q}(t) = [x_t(t), y_t(t), l(t), \varphi_x(t), \varphi_y(t)]^T, \quad (19)$$

substituting (16) in (17), and using the Lagrangian $L = T - V$, the nonlinear second order differential equation

$$\frac{d}{dt}\left(\frac{\partial L}{\partial \dot{q}_i(t)}\right) - \frac{\partial V}{\partial q_i(t)} = \frac{\partial Q}{\partial(\delta q_i(t))}, \quad (20)$$

can be resolved for $\ddot{\boldsymbol{q}}(t)$ and written as a first order ODE with the state vector $\boldsymbol{x}(t) = [\boldsymbol{q}(t), \dot{\boldsymbol{q}}(t)]^T$ and the vector of input forces $\boldsymbol{u}(t) = [F_x(t), F_y(t), F_l(t)]^T$ in form (1). Due to space limitations, the explicit outline of $\boldsymbol{f}(\cdot)$ is omitted here. Furthermore, it can be shown that the positions of the payload

$$\boldsymbol{y} = \begin{bmatrix} x_p \\ y_p \\ z_p \end{bmatrix} = \begin{bmatrix} h_x(\boldsymbol{x}) \\ h_y(\boldsymbol{x}) \\ h_z(\boldsymbol{x}) \end{bmatrix}. \quad (21)$$

are the flat output of system (16).

4.2 Feed Forward Control

Calculating the Lie-Derivatives Isidori (1995) of the flat output $\boldsymbol{y}$ yields a vectorial relative degree of

$$\boldsymbol{r} = \{r_x = 4,\ r_y = 4,\ r_z = 2\}$$

and the three ODEs

$$x_p^{(4)} = f_{x_p^{(4)}}(\boldsymbol{x}, F_x), \quad (22a)$$

$$y_p^{(4)} = f_{y_p^{(4)}}(\boldsymbol{x}, F_y), \quad (22b)$$

$$z_p^{(2)} = f_{z_p^{(2)}}(\boldsymbol{x}, F_l), \quad (22c)$$

which can be solved analytically for F_x, F_y and F_l. Similar results are already presented by Fliess et al. (1991) for the 2D-case. The diffeomorphism $\boldsymbol{\phi}(\boldsymbol{x}(t))$, transforming the physical coordinates $\boldsymbol{x}$ into flat coordinates $\boldsymbol{z}$ of the gantry, crane yields

$$\boldsymbol{z} = \boldsymbol{\phi}(\boldsymbol{x}) = \begin{bmatrix} h_x(\boldsymbol{x}) \\ h_y(\boldsymbol{x}) \\ h_z(\boldsymbol{x}) \\ \dot{h}_x(\boldsymbol{x}) \\ \dot{h}_y(\boldsymbol{x}) \\ \dot{h}_z(\boldsymbol{x}) \\ h_x^{(2)}(\boldsymbol{x}) \\ h_y^{(2)}(\boldsymbol{x}) \\ h_x^{(3)}(\boldsymbol{x}) \\ h_y^{(3)}(\boldsymbol{x}) \end{bmatrix}. \quad (23)$$

From (23), the inverse diffeomorphism $\boldsymbol{\phi}^{-1}(\boldsymbol{z})$ can be determined symbolically.

4.3 Trajectory Planning

In order to demonstrate the proposed methods for analytical multi-point trajectory planning, three intersection points for a movement of the load in the $x - y$ plane of the gantry crane with boundary conditions introduced in Section 3 of the form $\boldsymbol{P_{jz}} = [z_j, \dot{z}_j, \ddot{z}_j]$ are chosen as

$$\begin{array}{lllllll} \boldsymbol{P}_{1x} & = & [0.0, 0, 0] & & \boldsymbol{P}_{1y} & = & [0.0, 0, 0] \\ \boldsymbol{P}_{2x} & = & [0.07, 0.2, 0.34] & & \boldsymbol{P}_{2y} & = & [0.055, 0.17, 0.27] \\ \boldsymbol{P}_{3x} & = & [1.0, 0, 0] & & \boldsymbol{P}_{3y} & = & [0.8, 0, 0]. \end{array} \quad (24)$$

Since the load position (21) is a flat output, explicit dynamic constraints for the movement in x- and y-direction of the form $\boldsymbol{c}_z = \{\dot{z}^*_{max}, \ddot{z}^*_{max}, \ldots, z^{(n)*}_{max}\}$ (8) are formulated as

$$\boldsymbol{c}_x = \{1, 1, 1\} \qquad \boldsymbol{c}_y = \{0.4, 0.5, 0.5\}.$$

The numerical values are chosen such that existing physical constraints of the experimental gantry crane are kept and the introduced trajectory layout in the resulting feedforward trajectories can be verified easily.

The elements of the vectorial relative degree $\{r_x = 4,\ r_y = 4\}$ allow for a choice of $n = 4$ as smoothness parameters for the transition polynomials in (12).

Using the trajectory generation methods described in Section 3 for the intersection points (24) under consideration of the dynamic constraints (4.3), the trajectories presented in Figure 6 are achieved. Hereby, the overall traveling time of the x-axis was prolonged to the traveling time of the y-axis to achieve a synchronous movement in both directions. Note that due to the chosen boundary conditions in (24) the two segmented trajectories between $\boldsymbol{P}_1 \rightarrow \boldsymbol{P}_2$ and $\boldsymbol{P}_2 \rightarrow \boldsymbol{P}_3$ consist of only phase $\{I.1\}$ and $\{I.2,\ c,\ II.1,\ II.2\}$, respectively. The transition times T_{1c} and T_{2c} are equal to zero in both transition profiles.

4.4 Measurment results

Substituting the state vector in the inverse functions of (22) by the reference trajectories shown in Figure 6, the feedforward input vector $\boldsymbol{u}_{ff} = [F_x\, F_y\, F_z]$ can be computed. Measurement results of the corresponding trolley force $F_x(t)$ and the resulting load position $x_p(t)$ are shown in Figure 7. In the experimental setup, the gantry crane is equipped with frequency converted asynchronous motors operating in a speed regulated mode. Therefore, the computed feedforward trolley velocities $\dot{x}_t^*(t)$ and $\dot{y}_t^*(t)$ as well as the rate of change of the rope length $\dot{l}^*(t)$ are used as set values for the underlying motor controllers. In addition a load sway damping state feedback controller

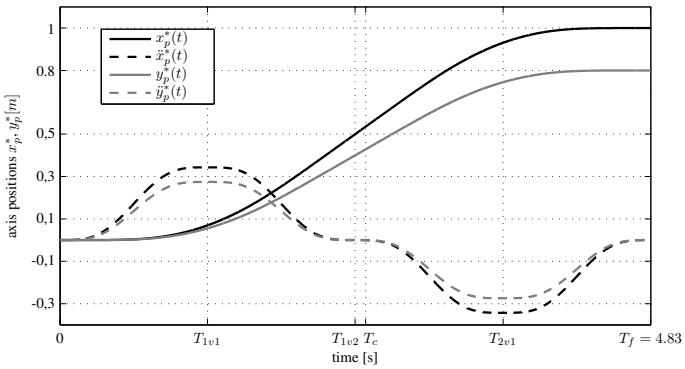

Fig. 6. Computed trajectories $x_p^*(t)$ and $y_p^*(t)$ with corresponding second order time derivatives for a three-point transition including two stages of segmented transition polynomials.

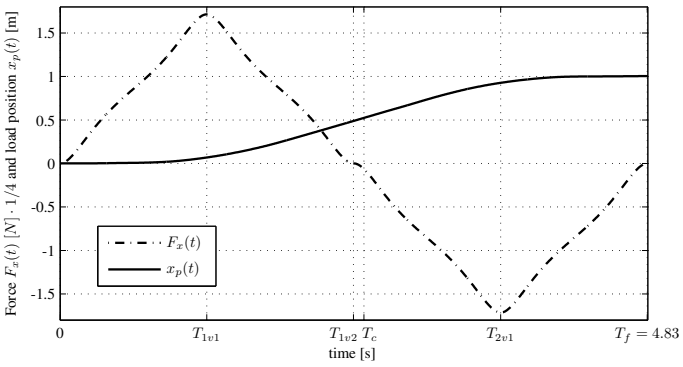

Fig. 7. Resulting feedforward force $F_x(t)$ and measured load position $x_p(t)$ (for visualization purposes the force was scaled by factor 1/4).

$\Delta \boldsymbol{u} = \boldsymbol{K}(\boldsymbol{x}(t))$ is used to achieve trajectory tracking to the desired multi-point trajectories $x_p^*(t)$ and $y_p^*(t)$ under external disturbances.

5. CONCLUSIONS AND FUTURE WORKS

Even though the theory presented in this paper is applicable to a more general structure of dynamical systems, for the special class of flat systems near time optimal trajectories can be computed analytically including explicit output constraints. By using a design parameter n, the smoothness of the trajectories can be adjusted to be n-times continuously differentiable. Both time scaling methods and applicability to discrete time systems are given such that segmented transition polynomials can be used in a wide field of control application. The flatness based feedforward control with segmented transition polynomials shows good results for an experimental 3-DOF gantry crane. For the movement of the crane load, a 4-times continuously differentiable trajectory is derived for two involved axes with different output constraints. Using time scaling methods derived in this paper, a synchronous movement along the computed trajectories is achieved.

In the current setup, an appropriate choice of boundary conditions $\boldsymbol{P}_j$ is assumed. However, including geometric constraints of the path planning process, the trajectory generation is effected. Further work on how to determine practical boundary conditions for use with segmented transition polynomials can lead to geometric path planning based on segmented polynomials in multiple dimensions.

REFERENCES

Barrère, R. and Carmasol, A. (1995). Approximate solutions of boundary-value problems using computer algebra software. *Mathematics with vision, Computational Mechanics Publications*, 45–52.

Canny, J., Rege, A., and Reif, J. (1991). An exact algorithm for kinodynamic planning in the plane. *Discrete and Computational Geometry*, 6, 461–484.

Choset, H., Lynch, K., Hutchinson, S., Kantor, G., Burgard, W., Kavraki, L., and Thrun, S. (2005). *Principles of robot motion*. MIT Press.

Craig, J.J. (1989). *Introduction to Robotics: Mechanics and Control*. Addison-Wesley Longman Publishing Co., Inc., Boston, MA, USA.

Donald, B., Xavier, P., Canny, J., and Reif, J. (1993). Kinodynamic motion planning. *Journal of the ACM*, 40, 1048–1066.

Fliess, M., Lévine, J., Martin, P., and Rouchon, P. (1995). Flatness and defect of non-linear systems: introductory theory and examples. *International Journal of Control*, 61(6), 1327–1361.

Fliess, M., Levine, J., and Rouchon, P. (1991). A simplified approach of crane control via a generalized state-space model. In *Proc. 30th IEEE Conference on Decision and Control*, volume 1, 736–741. doi:10.1109/CDC.1991.261409.

Fortune, S. and Wilfong, G. (1988). *Planning constrained motion*. ACM, New York, NY, USA. doi: http://doi.acm.org/10.1145/62212.62256.

Graichen, K., Hagenmeyer, V., and Zeitz, M. (2005). A new approach to inversion-based feedforward control design for nonlinear systems. *Automatica*, 41(12), 2033 – 2041. doi: DOI: 10.1016/j.automatica.2005.06.008.

Isidori, A. (1995). *Nonlinear Control Systems*. Springer.

Keller, H. (1976). Numerical Solution of Two Point Boundary Value Problems. *Society for Industrial Mathematics*.

Latombe, J. (1991). *Robot Motion Planning*. Kluwer Academic Publishers.

Lozano-Pérez, T. and Wesley, M. (1979). An algorithm for planning collision-free paths among polyhedral obstacles. *Communications of the ACM*, 22(10), 560–570.

Piazzi, A. and Visioli, A. (2001). *Optimal noncausal set-point regulation of scalar systems*, volume 37. Elsevier Ltd.

Ruppel, T., Zimmert, N., Zimmermann, J., and Sawodny, O. (2008). Kinodynamic planning-an analytical approximation with Cn polynomials for industrial application. *Control Applications, 2008. CCA 2008. IEEE International Conference on*, 528–533.

Sciavicco, L. and Siciliano, B. (2005). *Modelling and Control of Robot Manipulators (Advanced Textbooks in Control and Signal Processing)*. Advanced textbooks in control and signal processing. Springer, 2nd edition.

Sonneborn, L. and Van Vleck, F. (1964). The Bang-Bang Principle for Linear Control Systems.

Visioli, A. (2001). Trajectory planning of robot manipulators by using algebraic and trigonometric splines. *Robotica*, 18(06), 611–631.

von Stryk, O. and Bulirsch, R. (1992). Direct and indirect methods for trajectory optimization. *Annals of Operations Research*, 37(1), 357–373.

Zimmert, N., Sawodny, O., Arnold, E., and Oschmann, S. (2006). An on-line trajectory generation based on a model predictive approach. In *6^{th} Asian Control Conference*, 946–951. Bali, Idonesia. ISBN 979-15017-0.